Design and Fabrication of a Low Cost, Push Mode Piezoelectric Stream Droplet Generator with Interchangeable Nozzle

João Cardoso*[1], Cátia Moura[1], Daniela Ribeiro[1], Daniel Vasconcelos[1], Jorge Barata [1], André Silva[1]

[1]AEROG-LAETA, University of Beira Interior, Covilhã, Portugal
*Corresponding author email: joao.cardoso@ubi.pt

Abstract
The interest in studying droplet related phenomena has been increasing over the last decades. In the fluid dispensing equipment industry, a major problem is to minimize droplet diameter and to eject droplets in a controlled manner with a low-cost device. Taking all this into account, a new low-cost droplet stream generator was designed and fabricated. The material used to manufacture the stream droplet generator structure was a 3D printable material, namely PLA, that minimizes the device cost. This structure has three separate components: piezoelectric lid, fluid chamber, and pinhole holder. The disruptive waves of the disturbance mechanism were applied directly to the fluid instead of being applied to the precision pinhole. The interchangeable nozzle used was a round stainless-steel high precision optical pinhole with three different sizes: $100\ \mu m$, $150\ \mu m$, and $200\ \mu m$. Jet attribute properties (droplet diameter, droplet velocity, and distance between droplets) were measured as the different conditions changed (piezoelectric cell frequency, outlet pressure, and fluid). The present work studied the spray characteristics and different monodisperse regimes. A full characterisation of them is presented and discussed in detail.

Keywords
Monodisperse Regime, Stream Jet, Piezoelectric Droplet Generator, Rayleigh Breakup

Introduction

The interest in devices that produce small droplets with controlled size was initially developed to improve the resolution of ink-jet printing. Since then, the applications of this kind of device have been expanded to other areas such as biotechnology and manufacturing engineering, as well as for combustion applications [1]. In line with the problematic of gas emissions in the aviation sector, the use of biofuels is seen as one of the alternatives for the typical aviation jet fuel. Thus, it is important to study the differences between those fluids in an attempt to introduce them in internal combustion engines [2].

The process of jet disintegration is important for the design of plain-orifice atomizers and can be described by a bulk of liquid being converted into small droplets. One of the most elementary forms of atomisation is characterised by the formation of droplets by a slow emission of a liquid from a nozzle, forming a pendant droplet that grows slowly, which is characterised by a balance between inertial and surface tension forces. This mechanism can be associated as dripping and typically produces large droplets at low production rates [3]. When the liquid flow rate is progressively increased, increasing the liquid velocity, a continuous jet is formed. While emanating from a nozzle into an ambient gas, the liquid/gas interface is deformed, and the surface tension forces may tend to bring it back to the equilibrium shape, rising disturbances on the jet surface and, under certain conditions, amplifying the disturbances and disintegrating the liquid into droplets. This process of droplet formation is referred to as Rayleigh breakup. Rayleigh [4] obtained an expression for the resulting droplet size to a maximum instability, $D_d = 1.89d$, where D_d is the droplet diameter and d is the jet diameter, which is frequently considered the same as the nozzle diameter. Therefore, the average droplet size for the Rayleigh breakup

mechanism is almost twice the diameter of the undisturbed jet. A new diameter value for the droplets generated with this mechanism was later obtained by Tyler [5] in his experimental studies, where he obtained $D_d = 1.92d$. Similar to Rayleigh, Tyler found that this value can be obtained for the maximum instability. Weber [6] extended Rayleigh analysis to include viscous liquids. He found that the effect of the liquid viscosity is to shift the fastest growing waves to longer wavelengths and to slow down their growth rate, without, however, altering the value of the minimum wave number that makes the jet unstable. This means that the viscosity damps the instability growth, leading to the conclusion that the perturbations in fluids with high viscosity have a smaller growth rate than in fluids with low viscosity.

When the liquid velocity is further increased, the aerodynamic effects can no longer be neglected and can accelerate the breakup process. At still higher velocities, we enter the atomisation regime characterised by the appearance of a spray. Haenlein [7] identified four different regimes of breakup in the disintegration of a liquid jet. The first regime is the droplet formation without the influence of air, that is to say, the mechanism studied by Rayleigh. The second regime is characterised by a droplet formation with air influence. In this regime, the aerodynamic forces of the surrounding air are no longer negligible. In the third regime, the droplet formation is obtained due to the waviness of the jet and it is associated with an increase in the aerodynamic forces. The last regime is the complete disintegration of the jet.

The analysis on the jet formation process can be aided by some dimensionless governing parameters. The first relevant dimensionless number is the Reynolds number ($Re = \rho U_0 a/\mu$), where ρ is the fluid density, U_0 is the jet mean velocity, a is the length scale (e.g. droplet diameter or nozzle diameter) and μ is the fluid dynamic viscosity. This number represents the ratio between the inertial and viscous forces. Another relevant dimensionless number is the Weber number ($We = \rho {U_0}^2 a/\sigma$), where σ is the liquid surface tension. The Weber number represents the ratio between the inertial and surface tension forces. Combining the previous two numbers, in order to eliminate the velocity, results in the Ohnesorge number ($Oh = \sqrt{We}/Re = \mu/\sqrt{\rho\sigma a}$). The Ohnesorge number represents the influence of the fluid properties. Low Ohnesorge numbers represent either a low viscosity or a high surface tension.

The main objective of the present work is to introduce the design and fabrication of a low-cost droplet generator and validate its operation with the characterisation of the monodisperse regimes for three different fluids. The essential feature of these generators is to accurately control the size of the of the droplets and the spacing between them, obtaining a monodisperse regime. The main physical principle used to control these parameters is the Rayleigh breakup, explained previously. The performance of any type of atomiser depends on its size and geometry, as well as the ambient conditions and the liquid physical properties, while the flow and spray characteristics of most atomisers are strongly influenced by the liquid properties: surface tension, density and viscosity. For plain-orifice pressure nozzles specifically, the orifice diameter is the most important factor for atomisation and has great influence on the jet velocity and droplet diameter [1]. These devices are important tools for applications such as mechanical droplet-droplet interactions, impact of droplets on solid surfaces or liquid films, droplet evaporation, and validation of particle sizing techniques. However, many of the droplet generators available on the market are too expensive or cannot be used in certain applications.

Material and Methods

Droplet Generator Design and Fabrication

The device was designed using the CAD software CATIA v5 where all the parts were drawn separately and then assembled together to ensure all measurements were correct. The device has four different parts: superior lid part (Figure 1a), inferior lid part (Figure 1b), body (Figure 1c) and pinhole holder (Figure 1d) that were inspired in a previous work [8]. The superior lid part is the top part of the dispenser has the objective of pushing the inferior lid part against the body, sealing the device. The inferior lid part has the function of sealing the fluid chamber

located in the body part. Thus, the body part is the central part of the droplet generator by allocating the fluid chamber, establishing the connection between the liquid chamber and the pinhole holder, and supporting the piezoelectric diaphragm. The piezoelectric diaphragm was placed above the liquid chamber in order to generate disturbances directly onto the liquid surface in a parallel direction, making this device a push mode generator. This component was acquired from STEMINC, with the part number SMPD3SD35T25F18, and consists of a round piezoelectric ceramic plate which has electrodes on both sides and a single metal plate. Two copper wires are weld to both of them, allowing the external signal to excite the piezoelectric diaphragm. Finally, as the name suggests, the pinhole holder part main function is to hold the device pinhole, that function as a nozzle for the droplet generator. The interchangeable nozzle used was a round stainless-steel high precision optical pinhole with three different inner diameters: $100\ \mu m$, $150\ \mu m$, and $200\ \mu m$. Since the pinhole holder component is separated from the liquid chamber, the nozzle can be easily changed, enabling the cleaning/unclogging of the nozzle or allowing the exchange between nozzle sizes. All the parts described were assembled together, resulting in the device presented in Figure 2. The assemble of the device is divided into two different groups: piezoelectric ensemble and nozzle ensemble. Initially, a medical tube was inserted and glued to the admission hole located in the body part, as seen in Figure 2. After that, an O-ring was placed in the body upper hole to accommodate the piezoelectric diaphragm, which is wrapped in a water resistant material before the placement in the body part. After placing the piezoelectric, the superior and inferior lid parts are mounted together and placed above the body part, passing the copper cables inside the holes. Then, the structures (both lid parts) are assembled to the body part using bolts and nuts, finishing the assemble of the piezoelectric ensemble. Thereafter, the O-ring is aligned with the pinhole holder part and the stainless steel pinhole is placed in the pinhole holder hole between two small O-rings. Finally, both parts are assembled with nuts and bolts. The second ensemble (nozzle) must be disassembled after every use, while the first ensemble must be kept assembled with the exception of some maintenance processes.

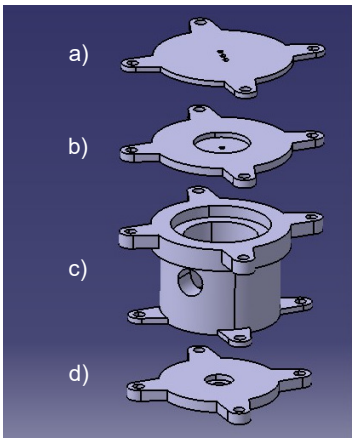

Figure 1. Droplet Generator parts; a) Superior Lid; b) Inferior Lid; c) Body; d) Pinhole holder.

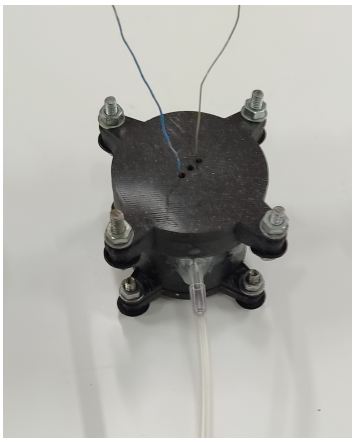

Figure 2. Droplet Generator Fully Assembled.

The parts described previously were all printed using the 3D printer Prusa i3 MK3. Two different 3D printable materials were used in the fabrication process: PLA and FilaFlexible40. PLA (Polylactic acid) is a renewable and biodegradable material with good thermomechanical properties and FilaFlexible 40 is a flexible and rubber-like material. Three different parts were printed using PLA: body, superior lid, and pinhole holder. As stated before, the superior lid part function is to push the inferior lid part, closing the device. Therefore, this part needs to have good mechanical properties to meet its purpose without changing its geometry. On the other hand, the body component has to contain the liquid chamber that suffers high internal pressure, thus a rigid material with good mechanical properties is needed. Lastly, the pinhole holder must

maintain its geometry so the final assemble could be performed successfully. For the parts that need to be flexible, FilaFlexible 40 was the chosen material. The inferior lid part was printed with this material since this part acts not only as a structural part but also as a sealant, thus, it needs to be flexible in order to seal the device. The other parts printed with this material, the O-rings, act as sealants and are used between the rigid parts.

Experimental Arrangement

An experimental setup was designed and built to obtain the validation of the device. This setup can be divided in four parts: image acquisition system, dispensing system, lighting setup and disturbance source. For the image acquisition system, an assembly of a high-speed digital camera and a macro lens was used, assuring results with high precision and quality. The values of time exposure (shutter) and frame rate were set at 1/80000 s and 25000 fps, lowering significantly the resolution to 1280x96 px^2 for the most part of the experiments. However, when the $100\ \mu m$ pinhole was used with a high flow rate, the resolution was even lower than before, since the shutter and frame rate used were 1/160000 s and 40000 fps, leading to a resolution of 1280x56 px^2. This was necessary because a large number of images is needed for the velocities calculation and the shutter plays a significant role when capturing images of moving objects. The dispensing system is the key to create the droplet stream and to select what types of conditions one might use. Three different components are part of this system: droplet generator, syringe pump, and medical tubes. The syringe pump is connected to the droplet generator through medical tubes, transporting fluid to the device and it was used to control the intake flow rate, employing different flow rates according to the different needs. Three different fluids were used in the experimental tests: distilled water (H_2O), jet fuel (JF), and a mixture of jet fuel and biofuel. The jet fuel chosen was Jet A-1 and the biofuel was NExBTL, a type of HVO (Hydroprocessed Vegetable Oil). The mixture has 50% in volume of jet fuel and 50% in volume of biofuel. The fluids properties were measured by Ribeiro et al. [9] and are presented in Table 1.

Table 1. Water, jet fuel and a jet fuel and biofuel mixture respective properties: surface tension, density and viscosity [9].

Fluid	Fluid properties		
	$\sigma\ [mN/m]$	$\rho\ [kg/m^3]$	$\mu\ [Pa.s]$
H_2O	71.97	1000.0	0.001003
100% JF	25.37	798.3	0.001120
50% JF / 50% HVO	24.64	792.4	0.001790

For the lighting setup, an halogen lighting unit was used behind a diffuse glass. The glass has the objective of diffusing and scattering the light. The disturbance source is formed by a piezoelectric diaphragm, a signal generator, and a picoscope tip. The signal generator allows the user to control different wave properties: shape, frequency, and amplitude. The signal created by the signal generator passes through the picoscope tip, which is then connected to the piezoelectric cell copper cable, enabling the piezoelectric diaphragm to excite.

Results and Discussion

In this chapter, the results obtained from the experiments will be presented. The experimental data was gathered using the experimental setup explained in the previous section, and the images were processed with a MATLAB algorithm that uses the Sobel filter for edge detection. In the initial tests, the piezoelectric diaphragm was not excited, allowing the visualisation of the free liquid jet, presented in Figure 3a. This jet is generated only by the device natural disturbances, which are originated by the pressure inside the fluid chamber. This process allows to understand the influence of the different parameters, such as fluid properties, pinhole

sizes and inlet flow rate, on the jet formation process. In Figure 3b, it is possible to observe the secondary droplets formation. In this regime, for each wavelength of an unstable disturbance, one main droplet and one or more, usually smaller droplets, referred to as satellite droplets, are generated. For this case in particular, for each regular droplet formation, a satellite droplet was generated. This pattern is a particular case for the secondary droplets formation and it was only observed when the auxiliary disturbance source (piezoelectric diaphragm) was enabled and it was mostly visualised for frequencies before the monodisperse cases. In Figure 3c it is possible to observe a monodisperse case. This regime is the most important for this study among all regimes obtained with the droplet generator and has two important characteristics: the droplets have the same diameter and they are equally distanced from each other. In order to generate a stream jet with these characteristics, all the natural disturbances were not sufficient to disturb the jet in a controlled Rayleigh-type jet breakup manner. Therefore, an additional disturbance source was needed so that the monodisperse regime could be reached. This disturbance source is obtained using the piezoelectric diaphragm at different wave frequencies. A particular case was found during the experiments and it can be observed in Figure 3d. This case represents the transition between different modes of disintegration and can be identified as a sinuous wave breakup, where the jet oscillates around its axis. This phenomenon was identified by Haenlein [7] and it is characterised by a drop formation due to the waviness of the jet. The aerodynamic forces are now more relevant in the droplet breakup process, while the surface tension is less relevant. The sinuous wave breakup was found only for a reduced number of tests and can be explained by the working conditions: small nozzle, relatively high flow rate and fluid properties that lead to a high velocity jet, entering in a new disintegration mode. All the cases presented in Figure 3 are examples of the regimes visualised in the testing process and all the regimes, except the sinuous wave breakup, were observed for all tested fluids and for all three pinhole sizes.

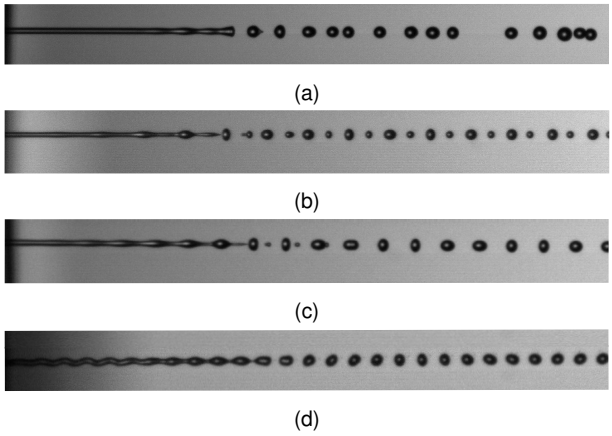

Figure 3. Visualisation of different regimes in the jet formation process; a) Free liquid jet formation; b) Secondary droplets formation; c) Monodisperse regime; d) Sinuous wave breakup.

Figures 4, 5, and 6 present a mathematical approximation for the droplet diameters to the cases that use a pinhole of $100\ \mu m$. The vertical lines limit the flow rate with the minimum and maximum values studied for these cases, which are $1.5\ ml/min$ for the minimum flow rate tested and $4.5\ ml/min$ for the maximum flow rate tested. The curves correspondent to the operational limits of the droplet generator were calculated using a quadratic polynomial regression, obtained with the experimental values from the testing phase. There were two sets of experimental values used in order to obtain the polynomial regression: the values with the lowest frequency that generated monodispersity and values with the highest frequency that generated monodispersity. The experimental values and their correspondent uncertainty values obtained with a confidence interval of 95% are represented in the graphs. Since the droplet diameter can vary with the flow rate and frequency, a linear approximation was calculated

with the values that were obtained with the same frequency and different flow rates, predicting for which values a certain frequency can be used. It is also possible to observe the droplet diameter limits expected by Tyler [5] experimental work and Rayleigh [4] theoretical work.
All three areas of operation obtained for the pinhole size of $100\ \mu m$ are different for each fluid and the range of values obtained with each fluid is different as well. However, all three fluids share a range of values from $206\ \mu m$ to $258\ \mu m$. Jet fuel was the only fluid that reached the diameter value predicted by Tyler [5], while in the water case, the values obtained were still far from that value. One could conclude that the maximum instability was achieved with complete success for the cases tested with jet fuel for high flow rates and the highest frequency to generate monodispersity. It was also noticeable that none of the cases reached the value predicted by Rayleigh [4], while some of them reached the experimental value predicted by Tyler [5].

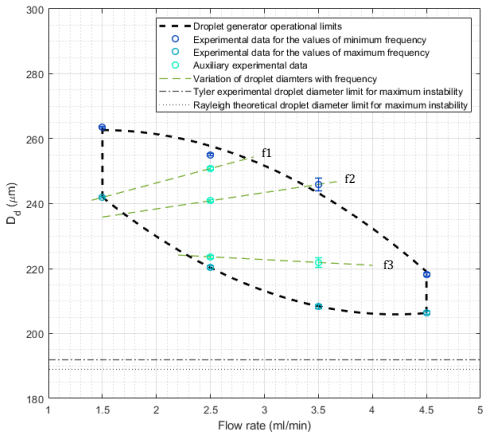

Figure 4. Mathematical approximation of the device operational droplet diameters using a pinhole of $100\ \mu m$ and water. Guidelines for different frequencies: $f1 = 7kHz$, $f2 = 9kHz$, $f3 = 11kHz$.

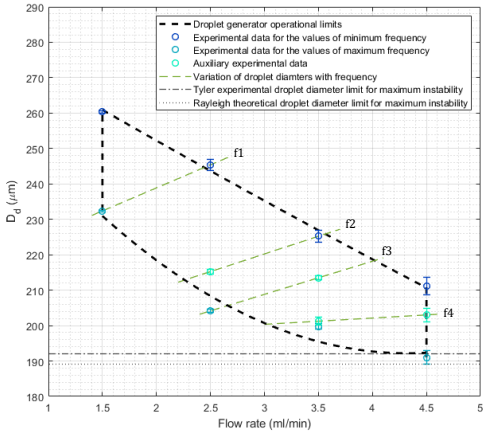

Figure 5. Mathematical approximation of the device operational droplet diameters using a pinhole of $100\ \mu m$ and jet fuel. Guidelines for different frequencies: $f1 = 9kHz$, $f2 = 15kHz$, $f3 = 19kHz$, $f4 = 22kHz$.

Figure 7 presents the jet velocity as a function of the inlet flow rate using a quadratic polynomial regression that was obtained using the experimental data for all three fluids and a pinhole size of $100\ \mu m$. Also, every experimental data has its correspondent uncertainty value, obtained with a confidence interval of 95%. It is possible to notice the differences between the jet fuel values and the other two fluids, given that jet fuel presents much higher velocity values than the other two fluids, while the fluid that exhibited lower velocity values was the jet fuel and biofuel mixture. The lower velocity values for the mixture can be explained by the role of viscosity in the jet disintegration process. Viscosity inhibits the growth of instabilities and delays the onset of disintegration, lowering the relative velocity.
Figure 8 shows the variation of the distance between droplets with frequency for the three different fluids. In order to achieve this, the experimental data was used to obtain the curve of tendency that shows this variation. Three cases are presented, one for each fluid, obtained using a pinhole size of $100\ \mu m$ and a flow rate of $2.5\ ml/min$. It is possible to observe that, for all fluids, the distance between droplets decreases with the increase of frequency. Despite of having different values, all fluids behave in a similar manner.
In figure 9, it is possible to observe the growth of the continuous jet with the inlet flow rate for three different fluids (water, jet fuel and a mixture of jet fuel and biofuel). All experimental data were acquired using a pinhole size of $100\ \mu m$. The first behaviour to notice is the increase of the continuous jet length with the increase in the flow rate for all cases. This can be explained by Savart [10] analysis: if the jet diameter is kept constant, the length of the continuous part of the jet is proportional to the jet velocity. It is also quite noticeable that the jet fuel presents higher

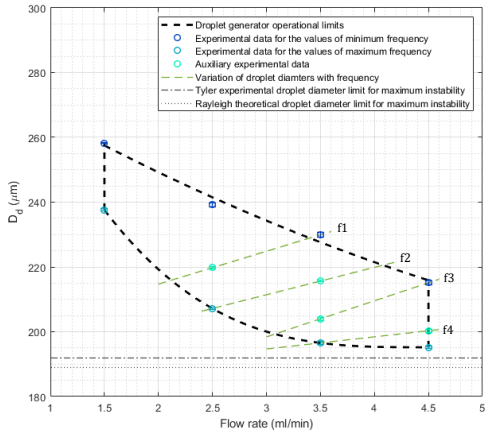

Figure 6. Mathematical approximation of the device operation droplet diameters, using a pinhole of $100\ \mu m$ and a biofuel and jet fuel mixture. Guidelines for different frequencies: $f1 = 8kHz$, $f2 = 10kHz$, $f3 = 12kHz$, $f4 = 14kHz$.

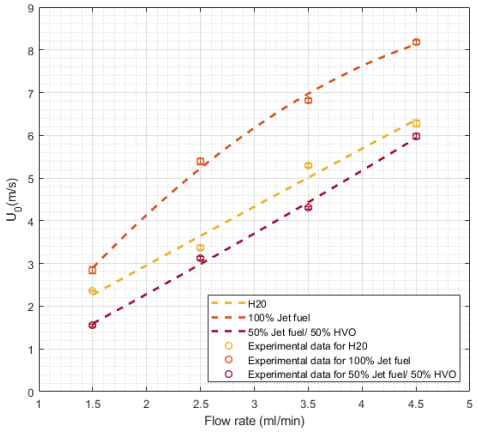

Figure 7. Mathematical approximation of the device operational jet velocity for a pinhole size of $100\ \mu m$.

values for all flow rates than the other two fluids, whereas water and the mixture have similar values. The difference between jet fuel and water can be explained by the difference in their surface tension values, since the Rayleigh jet breakup is caused by the growth of asymmetric oscillation of the jet surface, induced by the surface tension. Water surface tension is almost three times higher than jet fuel, allowing the jet to break up earlier, consequently generating a smaller continuous jet length. The same logic would be applied to the jet fuel and biofuel mixture because its surface tension is almost the same as the jet fuel. However, it is possible to observe that the continuous jet of the mixture has roughly the same length as the water case. This can be explained by the differences in the viscosity of these fluids. The mixture has a much higher viscosity than jet fuel and water (Table 1), hence it is not possible to apply the same logic to compare them since it is necessary to consider the fluids viscosity, in contrast to what was stated before. Weber [6] extended Rayleigh theory to include viscous liquids and with his work, it was possible to conclude that viscosity dampens the instability, reducing the continuous length for viscous liquids, explaining the continuous length difference between jet fuel and the mixture of jet fuel and biofuel. Then, it is possible to conclude that the mixture cannot be treated as an inviscid liquid in this analysis.

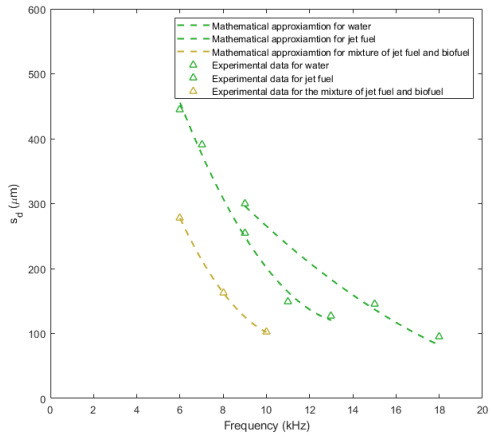

Figure 8. Variation of the distance between droplets with frequency for a pinhole size of $100\ \mu m$.

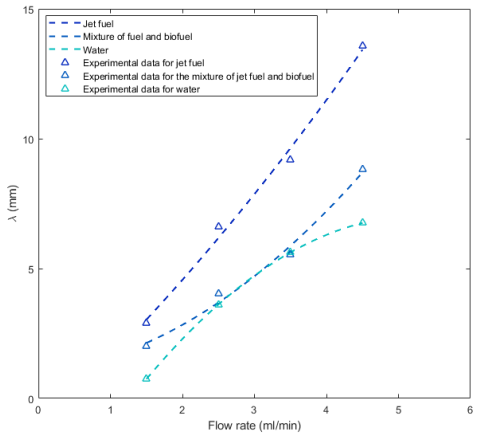

Figure 9. Continuous jet length growth for three different fluids with a pinhole size of $100\ \mu m$.

Conclusions

In this work, a stream droplet generator was designed, fabricated and validated. All the materials used to produce the device are cheap and simple to obtain, leading to the conclusion that it is possible to design and manufacture an affordable droplet generator and obtain jet disintegration for many regimes, conditions, and fluids.

It was possible to visualise different phenomena with the droplet generator, such as free liquid jet formation, monodisperse jet and satellite droplets. The monodisperse phenomena was analysed with more depth and the different jet properties were analysed. It was yet observed a sinuous wave, a particular case of a jet formation with the influence of aerodynamic forces.

It was noticeable that the jet fuel and biofuel mixture presented some differences when compared with jet fuel and distilled water, which can be explained by the high viscosity that this fluid presents. Given that biofuels are seen as one of the alternatives for the typical aviation jet fuel, it is possible to conclude that due to its properties, some of the processes inside the combustion chamber might be different from the typical jet fuel.

Acknowledgements

The present work was performed under the scope of Laboratório Associado em Energia Transportes e Aeronáutica (LAETA) activities, and it was supported by Fundação para a Ciência e a Tecnologia (FCT) through the project UIDB/50022/2020, and the grant sponsored by Fundação para a Ciência e a Tecnologia SFRH/BD/140009/2018 and SFRH/BD/143307/2019.

Nomenclature

a, d	Length scale $[\mu m]$, Nozzle diameter $[\mu m]$
D_d, f	Droplet diameter $[\mu m]$, Frequency $[kHz]$
Oh, Re, We	Ohnesorge number $[-]$, Reynolds number $[-]$, Weber number $[-]$
s_d	Distance between droplets $[\mu m]$
U_0	Jet velocity $[m/s]$
λ	Continuous jet length $[mm]$,
ρ, σ, μ	Density $[kg/m^3]$, Surface tension $[mN/m]$, Viscosity $[Pa.s]$

References

[1] Ashgriz, N., 2011, “Handbook of atomization and sprays: theory and applications”. Springer Science & Business Media.

[2] Ferrão, I., Vasconcelos, D., Ribeiro, D., Silva, A., and Barata, J., 2020, *Fuel*, 279, pp. 118321.

[3] Lefebvre, A. H. and McDonell, V. G., 2017, “Atomization and sprays”. CRC press.

[4] Rayleigh, L., 1878, *Proceedings of the London Mathematical Society*, 1, pp. 4-13.

[5] Tyler, E., 1933, *The London, Edinburgh, and Dublin Philosophical Magazine and Journal of Science*, 16, pp. 504-518.

[6] Weber, C., 1931, *ZAMM – Journal of Applied Mathematics and Mechanics*, 11, pp- 136-154.

[7] Haenlein, A., 1932, *Desintegration of a Liquid Jet*.

[8] Moura, C., 2020, “Design of a Monosized Droplet Generator”, Master Thesis.

[9] Ribeiro, D., Silva, A., and Panão, M., 2020, *Applied Sciences*, 10 (19), 6698.

[10] Savart, F., 1833, *Ann. Chim. Phys*, 53, pp. 337-386.